ADEOS-II/GLI ocean color atmospheric correction: early phase result

Hajime Fukushima*[a], Mitsuhiro Toratani[a], Akihiko Tanaka[b],
Wen-Zhong Chen[c], Hiroshi Murakami[c],
Robert Frouin[d], B. Gregory Mitchell[d], Mati Kahru[d]
[a]School of High-tech., Tokai University, Numazu, Japan 410-0395
[b]Nagasaki Industrial Promotion Foundation,
[c]National Space Development Agency of Japan Japan,
[d]Scrripps Institution of Oceanography

ABSTRACT

The paper presents initial results of atmospherically corrected ocean color data from the Global Imager (GLI), a moderate resolution spectrometer launched in December 2002 aboard ADEOS-II satellite. The standard GLI atmospheric correction algorithm, which includes an iterative procedure based on in-water optical modeling is first described, followed by brief description of standard in-water algorithms for output geophysical parameters. Ship/buoy-observed and satellite-derived marine reflectances, or normalized water-leaving radiance, are then compared, under vicarious calibration correction factors based on global GLI-SeaWiFS data comparison. The results, over 15 water-leaving radiance match-up data collected mostly off California and off Baja California, show standard errors in GLI estimate of 0.1 to 0.36 μW/cm^2/nm/sr for 412, 443, 490, and 565 nm bands, with improved standard errors of 0.09 to 0.14 μW/cm^2/nm/sr if *in situ* data set is limited to those obtained by in-water radiance measurement. Under provisional de-striping procedure, satellite-derived chlorophyll *a* estimates compares well with 35 ship-measured data collected off California within one day difference from the satellite observation, showing standard error factor of 1.73 (+73% or –43% error).

Keywords: satellite, remote sensing, validation, phytoplankton, chlorophyll a, CalCOFI, IMECOCAL, MOBY

1. INTRODUCTION

The Global Imager (GLI) was launched on December 14, 2002 aboard the Advanced Earth Observation Satellite II (ADEOS-II) by National Space Development Agency of Japan (NASDA). The instrument started its routine global observation in early April 2003. It has been under calibration initialization and initial validation phase until December 2003 when the distribution of version 1 standard products is supposed to commence.

Out of the 36 observation channels of GLI, up to about 10, extending 380 nm to 865 nm bands, could be used for ocean color remote sensing with 1 km spatial resolution at nadir. The instrument has a tilt mechanism to avoid the excess sunglint over the ocean. Detailed sensor specification and its initial status in orbit is described in Murakami *et al.*[1].

In this paper, we compare the GLI-derived and *in situ*-observed geophysical parameters in order
- to evaluate the soundness of the initial calibration,
- to verify the implementation of our atmospheric correction algorithm in the data processing system at NASDA Earth Observation Center (EOC), and
- to assess the performance of the standard atmospheric correction algorithm to help future updates and improvements.

After describing the standard atmospheric correction algorithm briefly, we compare the water-leaving radiances derived from the atmospherically-corrected GLI data with those measured during April 2003 cruises of California Cooperative Oceanic Fisheries Investigation (CalCOFI) and Investigaciones Mexicanas de la Corriente de California (IMECOCAL), in addition to the data obtained by the Marine Optical Buoy (MOBY) located off Lanai, Hawaii. Since the calibration initialization is still ongoing, we use several different sets of vicarious calibration numbers obtained by Yoshida *et*

* hajime@fksh.fc.u-tokai.ac.jp; phone 81 55 968-1111; fax 81 55 968-1155

al.(2003)[2] and Murakami *et al.*(2003)[1]. Satellite-derived chlorophyll *a* concentrations are also compared to the ship measurements acquired during the CalCOFI cruise.

2. GLI ATMOSPHERIC CORRECTION SCHEME

The standard GLI atmospheric correction is an extension of the OCTS algorithm (Fukushima *et al.,* 1998)[3] that shares the basis with the SeaWIFS algorithm proposed by Gordon and Wang (1994)[4]. For GLI, we have introduced an iterative procedure to take non-zero water reflectance in the near-infrared (NIR) bands into consideration, similarly to the one proposed by Siegel *et al.* (2000)[5] but taking the effects of inorganic suspended sediment and colored dissolved organic matter in addition to chlorophyll *a*. We have also updated the aerosol model set used in the atmospheric correction so that it minimizes unwanted discontinuity between pixels that may occur due to the pixel-wise selection of the aerosol model. Other improvements, such as sun-glitter and whitecap corrections, have been also implemented in the processing code but will not be discussed in this paper since they are still under evaluation or development.

2.1. Radiative transfer model equation

We assume that the following model equation holds for the satellite-observed radiance ρ_T for each pixel and for each observation band.

$$\rho_T(\lambda) = \rho_M(\lambda) + \rho_A(\lambda) + \rho_{MA}(\lambda) + t(\lambda)\rho_W(\lambda) \ , \qquad (1)$$

where λ is wavelength, ρ_M is the reflectance that would be observed from space when the atmosphere consists of gas molecules only, ρ_A is the reflectance that would be observed when the atmosphere comprises aerosol particles only, ρ_{MA} is the reflectance due to the interaction between molecules and aerosol particles, ρ_W is the reflectance of the ocean due to the back-scattering light that emerges from the water body, and t is the transmittance between ocean surface and the satellite. Note that the model equation here is expressed in terms of reflectance rather than radiance, although radiance L and reflectance ρ is easily converted with each other by the following relation.

$$\rho(\lambda) = \frac{\pi L(\lambda)}{F_0'(\lambda)\cos\theta_0} \ , \qquad (2)$$

where F_0' is extraterrestrial solar irradiance that takes two times of ozone absorption into account, and θ_0 is the solar zenith angle for that pixel.

2.2. General flow of the algorithm

The purpose of the atmospheric correction is to retrieve the water-leaving reflectance $\rho_W(\lambda)$ from given observed radiance $\rho_T(\lambda)$ for each pixel (see Eq. (1)). Knowing the atmospheric pressure at sea surface that comes from some objective analysis data, we can calculate the Rayleigh reflectance ρ_M with sufficiently good accuracy. The transmittance t can be also calculated with good accuracy. Thus, the only unknown term in Eq. (1) is $\rho_A + \rho_{MA}$. The general idea to do atmospheric correction is to estimate the magnitude of $\rho_A + \rho_{MA}$ in the shorter wavelength region from $\rho_A + \rho_{MA}$ in the NIR bands (670 ~ 865nm) where ρ_W, the water-leaving radiance is generally very low and can be discarded. That is, we get $\rho_A + \rho_{MA}$ at NIR bands by

$$\rho_A(\lambda) + \rho_{MA}(\lambda) = \rho_T(\lambda) - \rho_M(\lambda) \ . \qquad (3)$$

Estimating $\rho_A+\rho_{MA}$ for visible bands (380~ 625nm bands) is not straightforward since the spectral relation of $\rho_A+\rho_{MA}$ over the whole visible and NIR region is dependent on scan geometry. We use a look-up table that stores the relation between the aerosol reflectance $\rho_A+\rho_{MA}$ and aerosol optical thickness τ_A for each band and uses that table to determine the magnitude of $\rho_A+\rho_{MA}$ in the shorter wavelengths based on the estimated spectral ratio of τ_A between the two NIR bands. Specifically, since the relation between $\rho_A+\rho_{MA}$ and τ_A is also dependent on the aerosol type, the table is made to account for a set of aerosol models we assume for our algorithm.

The general flow to estimate $\rho_A+\rho_{MA}$ in shorter wavelength region is summarized as follows. First, based on the observed $\rho_A+\rho_{MA}$ in 670 (or 765) and 865 nm bands, we assume each of aerosol models to estimate τ_A for these bands in use of the aerosol reflectance *vs.* optical thickness table. Then, we select a pair of aerosol and, in use of the table again, estimate $\rho_A+\rho_{MA}$ in visible bands for each model, which is used to "synthesize" the $\rho_A+\rho_{MA}$ in each band. This brings us ρ_W, concluding the atmospheric correction.

Table 1. Aerosol models for GLI atmospheric correction.

Model No.	Aerosol Model	Number Mixture Ratio [%]		Relative Humidity [%]
		Tropospheric	Oceanic	
1	Tropospheric	100	0	70
2	Oceanic1600	99.9375	0.0625	70
3	Oceanic800	99.875	0.125	70
4	Oceanic400	99.75	0.25	70
5	Oceanic200	99.5	0.5	60
6	Oceanic200	99.5	0.5	73
7	Oceanic100	99	1	70
8	Oceanic50	98	2	70
9	Oceanic50	98	2	83

2.3. AEROSOL MODELS

GLI atmospheric correction has 9 candidate aerosol models as shown in Table 1. The definitions of these models are based on Shettle and Fenn (1979)[6], for example, the "Oceanic1600 type" consists of 99.9375% of tropospheric and 0.0625% (one 1600th) of oceanic aerosols, in terms of number of particles. RH means the assumed relative humidity. Other models are defined similarly.

2.4. Atmospheric correction with iteration

Due to saturation problems of the GLI nominal band16 (749nm) and band18 (865nm) even in non-cloudy ocean areas, GLI band13 (678nm) and band19 (865nm), were used for atmospheric correction. An iteration scheme is needed since these bands may be influenced by upward radiance from the sea. These near-infrared (NIR) water-leaving radiances should be corrected before atmospheric correction by using specific in-water model.

We developed an iterative procedure that corrects atmospheric effect with iteration to avoid the black pixel assumption. As shown in Figure 1, the water reflectance at near infrared bands are first estimated by using in-water model assuming initial values for chlorophyll *a* (*chl*) and inorganic suspended matter (*ism*) concentrations as well as absorption coefficient of colored dissolved organic matter (*cdom*). First atmospheric correction is executed, and new *chl*, *ism* and *cdom* are estimated by using neural network in-water algorithm. After the first atmospheric correction, the new water-leaving reflectance is estimated from obtained *chl*, and the second stage atmospheric correction is conducted. This process is repeated until *chl*, ism and *cdom* estimates converge.

2.4.1 In-water model at near infrared region

The in-water model for NIR water-leaving radiance is defined as follows

$$[\rho_w(\lambda)]_N = 0.533\pi R(\lambda)/Q, \qquad (4)$$

by Lee *et al.* (1994)[7] where λ is wavelength, and Q = 4.5 (Morel and Gentili, 1991)[8]. $[\rho_w(\lambda)]_N$ is normalized water- reflectance (Gordon, 1997)[9] given by

$$[\rho_w(\lambda)]_N = \rho_w(\lambda)/t_0,$$

where t_0 is the transmittance between sun and ocean surface. R is the reflectance just below surface and is defined by Joseph (1950)[10] as

$$R(\lambda) = \frac{\sqrt{1+2b_b(\lambda)/a(\lambda)}-1}{\sqrt{1+2b_b(\lambda)/a(\lambda)}+1}$$

where a and b_b is absorption and backward scattering coefficient, respectively. $A(\lambda)$ and $b_b(\lambda)$ are defined by

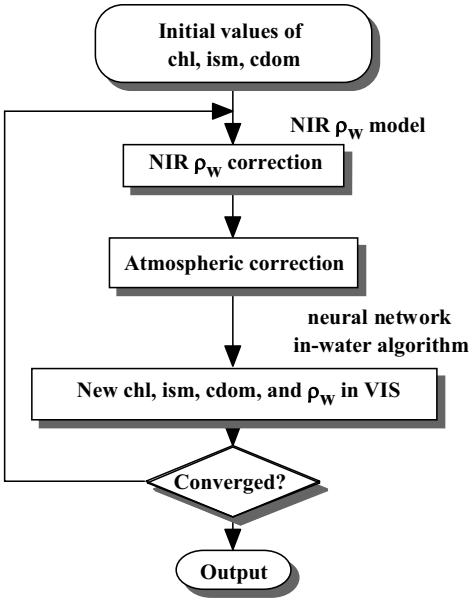

Figure 1. A simplified flow diagram of the pixel-wise GLI atmospheric correction with iteration. In the diagram, NIR and VIS stand for the near-infrared and visible bands, respectively.

$$a(\lambda) = a_w(\lambda) + a_c(\lambda, chl) + a_s(\lambda, ism) + a_y(\lambda), \text{ and} \quad (6)$$

$$b_b(\lambda) = b_{bw}(\lambda) + b_{bc}(\lambda, chl) + 2.7 \cdot b_{bs}(\lambda, ism) \quad (7)$$

where subscript w, c, s, y represents water, chlorophyll-a, inorganic suspended matter and yellow substance (*cdom*) respectively. Absorption coefficient values are given as follows.

$a_w(678) = 0.42829$, $a_w(865) = 4.6416$ by Pope and Fry (1997)[11]

$a_c(\lambda) = a_{cs}(\lambda) \cdot chl$ where *chl* is chlorophyll *a* concentration in mg/m^3

$a_{cs}(678) = 0.01968$, $a_{cs}(865) = 0$ by Kishino (personal comm.)

$a_y(\lambda) = a_y(440) \cdot \exp\{-0.014 \cdot (\lambda - 440)\}$ by Bricaud *et al.* (1981)[12]

The back scattering coefficients are given as follows:

$b_{bw}(\lambda) = 0.5 \times 0.00288 \cdot \left(\frac{\lambda}{550}\right)^{-4.32}$ by Morel (1974)[13]

$b_{bc}(\lambda) = 0.081 \cdot b_c(\lambda)$ by Oishi *et al*. (2002)[14]

$b_c(\lambda) = 0.27.chl^{0.698}.\left(\frac{\lambda}{550}\right)^{-0.2933}$ by Kishino (personal comm..)

$b_{bs}(\lambda) = b_s(\lambda) \cdot 0.01478$ by Babin and Doerffer (1996)[15]

$b_s(\lambda) = 0.125 \cdot ism \cdot \left(\frac{\lambda}{550}\right)^{-0.812}$ by Kronfeld (1988)[16]

2.4.2 Neural network-based in-water algorithm

A neural network is used for the iteration process to derive estimates of the chlorophyll-a concentration (*chl*), inorganic suspended solid concentration (*ism*) and absorption coefficient of colored dissolved organic matter (*cdom*) at 440nm (Tanaka *et al.*, 1998)[17]. The inputs for the neural net are the normalized water-leaving radiances at 412, 443, 460, 520, and 545 nm bands. These bands are chosen because they have high saturation radiances.

3. IN-WATER ALGORITHMS

GLI in-water algorithms were developed[18] for chlorophyll concentration (*chl*), diffuse extinction coefficient at 490nm (K490) and absorption coefficient of colored dissolved organic matter (*cdom*), and M. Kishino for suspended solids concentration (*ss*). The formulations used for GLI empirical algorithms were summarized in Table 2. For precise description, see http://suzaku.eorc.nasda.go.jp/GLI/ocean/algorithm/files/GLIOCEAN_algorithm.pdf.

3.1. Chlorophyll *a* algorithm

Simple band-ratio empirical algorithms were used for deriving standard products including *chl*, K490 and *cdom*. Previous *chl* algorithm was based on the CAL-P6 algorithm (Kahru and Mitchell,1999)[19] and used the ratio of normalized water-leaving radiances (see definition in section 4) at 490nm and 565nm ($nL_w(490)/nL_w(565)$). Due to the possible saturation problem at both of these GLI bands, the chl algorithm was changed to use a maximum-band-ratio (MBR) algorithm using the maximum of 3 bands ($nL_w(443)$, $nL_w(460)$ and $nL_w(520)$) with $nL_w(545)$ in the denominator.

3.2. K490 algorithm

The K490 algorithm was modified from previous version due to the possible saturation problem of the GLI 490 and 565 bands. The current K490 product is derived as a cubic function of $nL_w(460)/nL_w(545)$ in the log-log space. It provides better retrieval compared to the approach of SeaWiFS using $nL_w(443)/nL_w(555)$. Due to inherent variability in the K490 estimates in very clean waters, some K490 estimates that were below the estimated pure water values were excluded.

Table 2. Formulations of the GLI empirical algorithms.

Variable	Algorithm	Type	Equation
chl	OC4-GLI by Kahru and Michell., 1999 modified from O'Reilly *et al.,*1998	Max Band Ratio, Modified Cubic Polynomial	chl= $10^{(a0 + a1*R + a2*R^2 + a3*R^3 + a4*R^4)}$ +a5 R = $\log_{10}(nL_w(443) > nL_w(460) > nL_w(520) / nL_w(545))$
K490	GLI-K490 modified from Mitchell and Kahru, 1998	Cubic polynomial in log-log	K490 = $10^{(a0 + a1*R + a2*R^2 + a3*R^3)}$ R = $\log_{10}(nL_w(460)/nL_w(545))$
cdom	In preparation by Michell and Kahru	Linear band ratio in log-log	Cdom(440) = $10^{(a0 + a1*R)}$ R = $\log_{10}(nL_w(443)/nL_w(520))$
SS	Provided by Kishino, 2002	Band ratio, Quadratic in log-log	SS=$10^{(a0+a1*R+a2*R^2)}$, R=$\log_{10}(nL_w(443)/nL_w(545))$

3.3. Cdom absorption algorithm

For the cdom product all combinations of GLI band ratios were tested versus *in situ* measurements of $a_y(300)$, i.e. absorption coefficient of dissolved material at 300 nm. The best band ratio with the highest r^2 and lowest RMSE appeared to be $nL_w(380)/nL_w(545)$. Band ratios $nL_w(412)/nL_w(520)$, $nL_w(412)/nL_w(545)$ and $nL_w(443)/nL_w(520)$ were slightly but not significantly inferior. A large proportion of the scatter is actually due to measurement errors and not due to algorithm errors. Our experience with SeaWiFS (Kahru and Mitchell, 1999)[19] shows that atmospheric correction at short wavelengths in the coastal zone may have large errors. Therefore we did not select band ratios including short wavelength bands (380, 412 nm) for the *cdom* algorithm. As similar results can be achieved with other bands for which atmospheric correction should be more robust, we selected $nL_w(443)/nL_w(520)$. This ratio appears to be well correlated with *cdom* absorption due to the fact that a significant part of phytoplankton influence on this ratio tends to cancel out. Additional advantage of this band ratio (compared to band ratios using bands 380 and 400 nm) is that 443 and 520 nm bands are common on other sensors and the same algorithm can therefore be used on these sensors, provided that accurate nL_w values are available. The operational *cdom* definition is the amount of absorption by the dissolved organic component at a certain wavelength. We originally used the wavelength of $a_y(300)$ as a proxy to the concentration of *cdom* due to a better signal to noise ratio at this wavelength. At 440 nm wavelength the relative amount of measurement error is significantly higher which results in the reduction in r^2 of the estimate. Per request of Dr. Kishino and according to original NASDA plans, we are now providing algorithm for $a_y(440)$.

3.4. Suspended matter algorithm

It is extremely difficult to use traditional empirical method (*e.g.* band ratio) for coastal zone. The concentration of various materials, such as phytoplankton, organic or inorganic suspended matter and dissolved organic matter, should be considered. As a candidate, there is inversion method that inverses remote sensing reflectance or normalize water leaving radiance. However, its disadvantage is to take significant time to find solution. While neural network needs time to be educated, it can process data very quickly after educated. However, to the moment, the inversion accuracy is not satisfactory. For GLI, both empirical and neural network algorithms were developed to derive suspended solid concentration, and currently neural network algorithm was selected to derive standard product.

A database of suspended solid (SS) and chlorophyll concentrations for Case 1 waters was built and an empirical algorithm for SS concentration was developed. In this study, the database was built from the data measured by Tokyo University of Fisheries, National Polar Research Institute, RIKEN and Nagasaki University. PRR-600, MER-2040, PRR-800 (Biospherical Inc.) were used to measure in-water radiance/irradiance. From the database, the relationship between chlorophyll-a concentration and suspended solid was found. Normalized water leaving radiance was computed from remote sensing reflectance of the selected data. For all the GLI bands except 565 nm and 490 nm that can be saturated, the ratio to 545 nm band was computed. Correlation between the band ratio and SS concentration was computed.

SS concentration measurements may include considerable error from the spots in suspended solid itself and the foreign dusts, which differ from other measurements. As a result, the correlation is not so high. Algorithm should be improved

Table 3. *In situ* data sets and GLI scenes used in this study.

	# of collected ship/buoy data		# of satellite scenes		# of used match-up data	
	nL_w	chl	L1B	L2	nL_w	chl
CalCOFI 0304 PRR by Mitchell & Kahru	39		19		3	
CalCOFI 0304 SIMBAD by Frouin	71		19		5	
IMECOCAL 0304 SIMBAD by Frouin	79		8		4	
MOBY Feb.-May, 2003 by Clark	7		9		4	
CalCOFI 0304 Chl by CalCOFI program		90		21		35

with more truth data in future.

For Case 2 waters, with the advanced model of optical process, the algorithm for estimating both SS and dissolved organic matter should be established. For that purpose, the optical property measurement of various materials, the establishment of the relationship of optical property and in-water materials in various ocean areas are required.

4. EARLY PHASE VALIDATION

4.1. *In-situ* data set and quality control

Collected *in-situ* data sets, as summarized in Table 3, were obtained from two cruises and from MOBY mooring system. During CalCOFI0304 cruise off California in April 4-22, 2003, in-water and above water optical measurements were conducted aboard R/V *Roger Revelle*. Upwelling radiance at depth z, $L_u(z)$, was measured by PRR800 high resolution profiling reflectance radiometer in 18 spectral bands covered from 313nm to 710nm. The water-leaving radiance L_w was retrieved from $L_u(0^-)$, the upwelling radiance just beneath the ocean surface extrapolated to 0^- from $L_u(z)$ [Mitchell and Kahru, 1998]. Normalized water-leaving radiance nL_w was derived by

$$nL_w = 0.519 * L_u(0^-) * F'_0 / Ed(0^-),$$

where F'_0 is the extraterrestrial solar radiance and $E_d(0^-)$ is the downward irradiance just beneath the sea-surface, which was derived from in water $E_d(z)$ measurement in a similar way as $L_u(0^-)$ from $L_u(z)$. Water-leaving reflectance was also measured by a SIMBAD instrument built by the University of Lille in 5 spectral bands centered at 443, 490, 560, 670, and 870 nm, from which nL_w was estimated using calculated $E_d(0^+)$, downward irradiance above the sea-surface. SIMBAD measurements were also conducted on IMECOCAL0304 cruise off Baja California aboard R/V *Francisco de Ulloa* during April 8-22. Another set of water-leaving radiance data through February-April, 2003 was obtained from MOBY optical mooring system off Lanai Island, Hawaii, from which nL_w data was derived based on calculated $E_d(0^+)$.

During the CalCOFI0304 cruise, chlorophyll *a* concentrations were determined by the fluorometric method. For this study the averaged values over the first 10 m measurement.

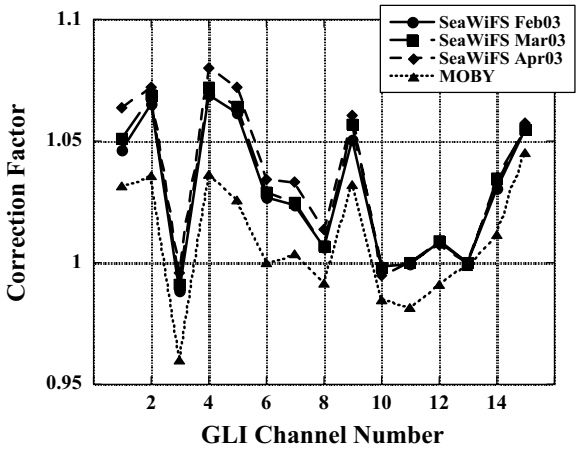

Figure 2. Calibration correction factors derived by vicarious calibrations based on SeaWiFS (Murakami *et al*., 2003)[1] or MOBY (Yoshida *et al*., 2003)[2]. Satellite vs. *in situ* nL_w comparisons are made for channels 3 (412 nm), 4 (443 nm), 6 (490 nm) and 9 (565 nm).

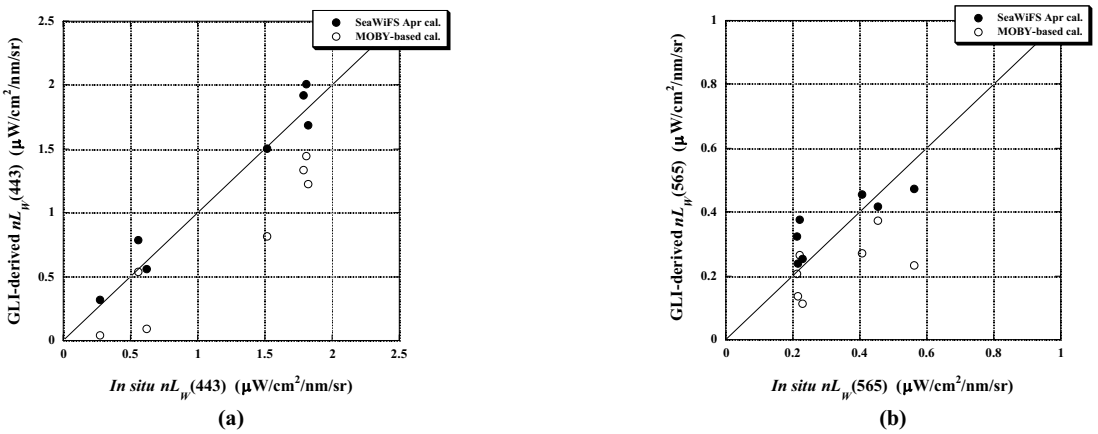

Figure 3. Effect of different calibration correction factors on *in situ*-based and GLI-derived normalized water-leaving radiances. In-water radiance data of PRR800 at CalCOFI0304 cruise and MOBY located off Lanai, Hawaii are used.

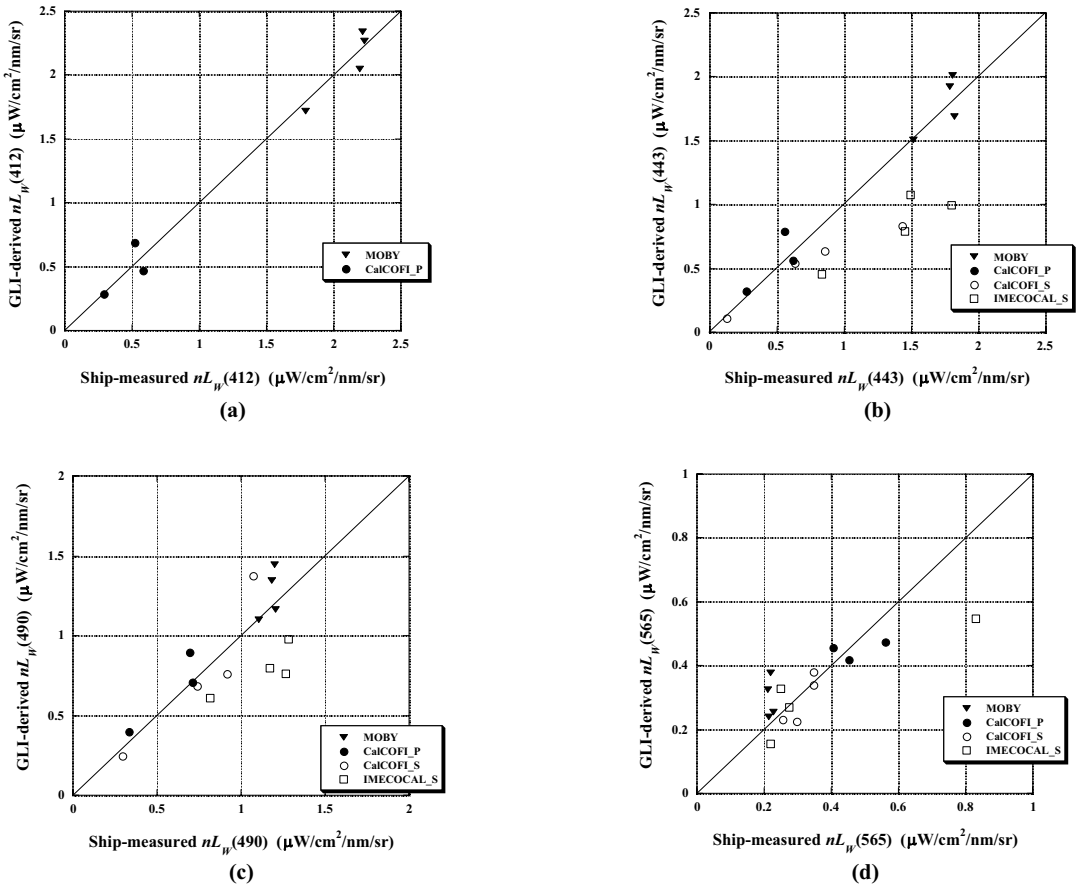

Figure 4. GLI-derived normalized water-leaving radiance (nL_W) compared to ship/buoy-based radiance for (a) 412 nm, (b) 443 nm, (c) 490 nm, and (d) 565nm bands. Solid symbols correspond to the in-water measurements (CalCOFI_P and MOBY) whereas open symbols correspond to SIMBAD (CalCOFI and IMECOCAL_S).

To leave the quality data for the match-up analysis, all the nL_w data with more than ±3 hour time difference with respect to the satellite observation time were screened out. For chlorophyll *a* match-up, time window was widened up to one day difference.

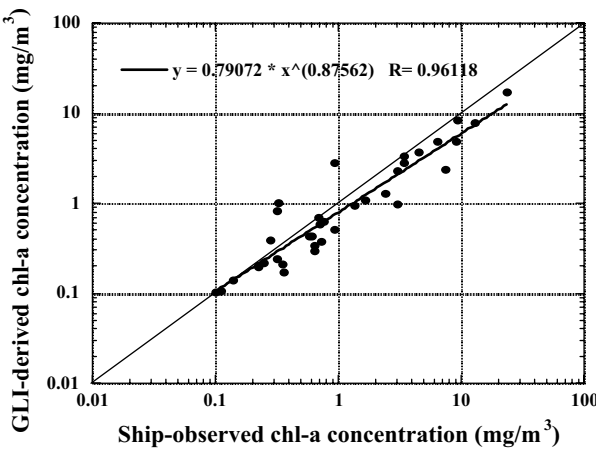

Figure 5. Comparison of ship-measured and GLI-derived chlorophyll *a* concentration over CalCOFI April 2003 cruise. "Match-up time window", or allowed time difference between ship and satellite observation is ± 1day.

4.2. GLI data processing

4.2.1. GLI data for nL_w match-up

Level-1 GLI match-up image data, each of which consists of 125 by 125 scene centered at the location of the ground measurement, were first converted into the total radiance data L_t assuming either of SeaWiFS-based[1] or MOBY-based[2] calibration factors shown in Figure 2. It was processed by the standard atmospheric correction, with the cloud screening threshold of $r_a(865) = 2.2$ %. Sun-glitter and whitecap corrections were not applied for this early stage analysis. Since preliminary analysis revealed significantly large striping noise[1] of 24 line cycle, we decided to apply 24 by 24 median filter to the L_t radiance data, which is to be fed into the atmospheric correction. With tentative atmospheric correction, we chose one out of 9 standard aerosol models for each image, which can best interpret the observed aerosol radiances at 670 and 865 nm bands. Derived nL_w image was filtered by 24 by 24 averaging to further reduce the noise level.

4.2.2. GLI chlorophyll *a* imagery

Since we judged the effect of striping noise is too large, an empirical, scene-wise optimized destriping procedure was applied to the GLI Level-1B data that covers the CalCOFI0304 area.

4.3. Effect of calibration correction factor on satellite-derived water-leaving radiance

To evaluate the effect of calibration correction factor, we applied four different correction factors shown in Figure 2 to produce nL_W image. Out of the four, three sets were derived by the global GLI-SeaWiFS vicarious calibration (Murakami *et al.*, 2003)[1], the other derived from vicarious calibration with MOBY (Yoshida *et al.*, 2003)[2]. Figure 3 is an example of the result of comparison of GLI-derived nL_w and those obtained by CalCOFI and MOBY in-water measurements, where aerosol optical thickness at 865 nm ranges from 0.05 to 0.2. As shown, the nL_w differences due to the SeaWiFS and MOBY-derived correction factors are about 0.5 and 0.2 μW/cm^2/nm/sr for 443 and 565 nm bands, respectively, with SeaWiFS-based one giving significantly less estimation error. Since similar superiority was observed for other bands, we choose the SeaWiFS-based correction factors for the rest of the analysis.

4.4. Match-up data analysis on water-leaving radiance

The match-up comparison results for nL_w at 412, 443, 490 and 565 nm bands are shown in Figure 4, where solid symbols mean that the *in situ* data was obtained by in-water measurements while the open symbols corresponds to the *in situ* nL_w obtained by the on-deck SIMBAD measurements. The standard error, or RMSE of GLI estimates against ship/buoy measurements ranges from 0.1 to 0.36 μW/cm^2/nm/sr for these bands. The error is reduced to 0.09 to 0.14 μW/cm^2/nm/sr if we exclude *in situ* nL_w data derived from SIMBAD instruments under preliminary calibration.

4.5. Satellite and ship chlorophyll *a* comparisons

With the criterion that ship observation be done on the same day as, or one day earlier or later from the satellite observation, 35 match-up data remained out of 90 CalCOFI chlorophyll *a* ship measurements. Figure 5 shows the comparison of GLI-derived estimates with ship-determinations. The satellite-derived chlorophyll *a* compares remarkably well, showing standard error factor (RMSE on log-scale) of 1.73 (+73% or –43% error).

5. CONCLUSION

As an initial validation, we compared GLI-estimates with early *in situ* data sets. Although the calibration initialization of the GLI instrument is still underway, and most ship-measured data are still preliminary status, the comparison shows

the soundness of the early GLI status and the promising possibility of GLI data application.

ACKNOWLEDGMENT

The authors express their thanks to the CalCOFI program who contributed in-situ chlorophyll-a data in a timely manner. They also wish to thank M. De la Cruz for making SIMBAD measurements during the IMECOCAL cruise and A. Poteau for processing the data. Thanks are extended to D. Clark who contributed MOBY-derived data and to A. Mukaida and his group at RESTEC who prepared the GLI match-up data set. This study was supported by the ADEOS-II/GLI Project at National Space Development Agency of Japan. R. Frouin and B. G. Mitchell are also supported by National Aeronautics and Space Administration and the SIMBIOS Project Office, which are gratefully acknowledged.

REFERENCES

1. H. Murakami, K. Tanaka, S. Kurihara, Y. Okamura, J. Inoue, J. Nieke, I Asanuma, H. Yatagai, Y. Mitomi, M. Yoshida, R Higuchi, S. Kawamoto, K. Isono, and Y. Senga, GLI early calibration results for oceanographic applications., *Proc.of Int. Sym. on Optical Science and Technology*, SPIE, 2003.
2. M. Yoshida, Y. Mitomi, Y. Senga, I. Asanuma, H. Murakami, K. Sasaoka, K. Sato, Early phase evaluations of GLI vicarious calibration factors for ocean color channels, *Proc. Int. Sym. Optical Science ant Technology* (2003).
3. H. Fukushima, A. Higurashi, Y. Mitomi, T. Nakajima, T. Noguchi, T. Tanaka, and M. Toratani, "Correction of atmospheric effect on ADEOS/OCTS ocean color data: Algorithm description and evaluation of its performance", *Journal of Oceanography*, Vol. 54, 417-430, 1998.
4. Gordon, H.R., and M. Wang, Retrieval of water-leaving radiance and aerosol optical thickness over the oceans with SeaWiFS: a preliminary algorithm, *Appl. Opt.,* **33**(3), pp. 443-452, 1994.
5. D. A. Siegel, M. Wang, S. Maritorena, and W. Ronbinson, Atmospheric correction of satellite ocean color imagery: the black pixel assumption, *Applied Optics*, 30, 21, 3582-3591, 2000.
6. E. P. Shettle, and R. W. Fenn, Models for the aerosols of the lower atmosphere and the effects of humidity variations on their optical properties, *AFGL-TR-79-0214*, 675, 94pp., 1979.
7. Z. Lee, K. Carder, S. Hawes, R. Steward, T. Peacock and C. Davis, Model for the interpretation of hyperspectral remote-sensing reflectance, Applied Optics, Vol.33, pp.5721-5732, 1944.
8. A. Morel and B. Gentili, Diffuse reflectance of oceanic waters : its dependence on sun angle as influenced by the molecular scattering contribution, Applied optics, 30, 4427-4438, 1991.
9. H. R. Gordon, Atmospheric correction of ocean color imagery in the Earth Observation System era, *J. Geophys. Res*., 102 (D14), 17,081-17,106, 1997.
10. Joseph, J., Untersuchungen über ober- und unterlichtmessungen im Meere und über ihren zusammenhang mit durchsichtigkeitsmessungen, Deut. Hydorograph. Z., Vol.3, pp.324-335, 1950.
11. R. M. Pope and E. S. Fry, Absorption spectrum (380-700) of pure water, II: Integrating cavity measurement, *Applied Optics*, Vol.36, pp.8710-8723, 1997.
12. A. Bricaud, A. Morel and L. Prieur, Absorption by dissolved organic matter of the sea (yellow substance) in the UV and visible domains, *Limnol. Oceanogr.*, Vol.26, No.1, pp.43-53, 1981.
13. A. Morel, Optical properties of pure water and pure sea water, chapter 1 in *Optical Aspects of Oceanography*, edited by N. G. Jerrov and E.S. Nielsen, Academic Press, New York, 1-24, 1974.
14. T. Oishi, Y. Takahashi, A. Tanaka, M. Kishino, and A. Tsuchiya, Relation between the backword- as well as total scattering coefficients and the volume scattering functions by cultured phytoplankton. *J. School Mar. Sci. Technol. Tokai Univ.*, Vol.53, pp.1-15 (in Japanese with English abstract), 2002.
15. M. Babin and R. Doerffer, Specifications for case II coastal water reference model., Algorithm Theoretical Basis Document for MERIS (ATBD 2.12), ESA-ESTEC, pp.61-73, 1996.
16. U. Kronfeld, Die optishen eignenschatten der ozea nischen shwebstoffe und ihre bedentung fur fernerkundung von phytoplankton., *GKSS Forschungszentrum*, D-2054 Geesthacht, Germany, 153 pp, 1988.
17. A. Tanaka, T. Oishi, M. Kishino, and R. Doerffer, "Application of the neural network to OCTS data", Proc. Ocean Optics XIV, S. G. Ackleson and J. Campbell (eds.), Office of Naval Research, Washington, D.C., 1998.
18. B. G. Mitchell and M. Kahru, Algorithms for SeaWiFS developed with the CalCOFI data set, *CalCOFI Rep. 39*, 26 pp., Calif. Coop. Oceanic Fish. Invest. Rep., Calif., 1998.
19. M. Kahru and Mitchell, B.G., Empirical chlorophyll algorithm and preliminary SeaWiFS validation for the California Current, *Int. J. Remote* Sensing, 20. 17., 1999.